Quantification of 3D macropore networks in forest soils in Touzhai valley (Yunnan, China) using X-ray computed tomography and image analysis

ZHANG Jia-ming[1] http://orcid.org/0000-0002-0695-9744; e-mail: zjm_engeo@163.com

XU Ze-min[1]* http://orcid.org/0000-0002-0092-4284; ✉e-mail: abc5100@188.com

LI Feng[2] http://orcid.org/0000-0002-7922-7245; e-mail: lifeng@kmust.edu.cn

HOU Ru-ji[3] http://orcid.org/0000-0002-3463-4410; e-mail: houruji2012@163.com

REN Zhe[1] http://orcid.org/0000-0001-8848-4211; e-mail: kmrz1204@163.com

Corresponding author

1 Department of Civil Engineering, Kunming University of Science and Technology, Kunming 650500, China

2 Department of Earth Sciences, Kunming University of Science and Technology, Kunming 650093, China

3 Water Transportation Planning and Design Institute of Yunnan, Kunming 650051, China

Citation: Zhang JM, Xu ZM, Li F, et al. (2017) Quantification of 3D macropore networks in forest soils in Touzhai valley (Yunnan, China) using X-ray computed tomography and image analysis. Journal of Mountain Science 14(3). DOI: 10.1007/s11629-016-4150-9

Abstract: The three dimensional (3D) geometry of soil macropores largely controls preferential flow, which is a significant infiltrating mechanism for rainfall in forest soils and affects slope stability. However, detailed studies on the 3D geometry of macropore networks in forest soils are rare. The intense rainfall-triggered potentially unstable slopes were threatening the villages at the downstream of Touzhai valley (Yunnan, China). We visualized and quantified the 3D macropore networks in undisturbed soil columns (Histosols) taken from a forest hillslope in Touzhai valley, and compared them with those in agricultural soils (corn and soybean in USA; barley, fodder beet and red fescue in Denmark) and grassland soils in USA. We took two large undisturbed soil columns (250 mm×250 mm×500 mm), and scanned the soil columns at in-situ soil water content conditions using X-ray computed tomography at a voxel resolution of $0.945 \times 0.945 \times 1.500$ mm³. After reconstruction and visualization, we quantified the characteristics of macropore networks. In the studied forest soils, the main types of macropores were root channels, inter-aggregate voids, macropores without knowing origin, root-soil interface and stone-soil interface. While macropore networks tend to be more complex, larger, deeper and longer. The forest soils have high macroporosity, total macropore wall area density, node density, and large macropore volume, hydraulic radius, mean macropore length, angle, and low tortuosity. The findings suggest that macropore networks in the forest soils have high inter-connectivity, vertical continuity, linearity and less vertically oriented.

Introduction

Preferential flow is a hydraulic phenomenon and a significant rainfall infiltration mechanism in forest soils (Sidle et al. 2001; Van Schaik et al. 2008; Legout et al. 2009; Wiekenkamp et al. 2016).

Preferential flow dominates the hydrological regime and affects slope stability, especially in steep forest watersheds in humid climate regions (e.g. Uchida et al. 2001; Anderson et al. 2009). Moreover, preferential flow has important effects on land degradation, soil erosion control, and on groundwater resource security (e.g. Hanson et al. 2004; Zhao et al. 2016; Zhang et al. 2016). However, macropores (such as animal burrows, decayed root channels, fissures and interaggregate voids) are important factors influencing preferential flow (Capowiez et al. 1998; Mooney 2002; Capowiez et al. 2011; Katuwal et al. 2015; Hu et al. 2015; Hu et al. 2016), even though they represent only a small fraction of the total soil volume (Lin et al. 1996; Alaoui and Helbling 2006; Holden 2009). Consequently, quantification of 3D macropores is essential to relate macropore characteristics to preferential flow behavior and to develop a reasonable mathematical model.

Up to now, many efforts have been carried out to visualize and quantify macropores in forest soils using either dye tracers technique (Schlather and Huwe 2005; Bogner et al. 2008; Anderson et al. 2009; Nobles et al. 2010; Zhang and Xu 2013; Laine-Kaulio et al. 2015), water break-through curve technique (e.g. Lu et al. 2014) or tension disk infiltrometer (Watson and Luxmoore 1986; Buczko et al. 2006; Holden 2009). However, these methods have limited ability to observe 3D macropore geometry and topology (e.g. Luo et al. 2010). With advances in image processing techniques (software & algorithms), X-ray computed tomography (XRCT) has been used in recent years as a non-destructively method to quantify 3D geometry and topology of macropores in undisturbed soil cores (e.g. Hu et al. 2015; Pagenkemper et al. 2015; Bottinelli et al. 2016) or sieved and repacked soil samples (e.g. Jégou et al. 2001; Capowiez et al. 2011) at a much higher resolution than the aforementioned methods. Several studies showed that XRCT is a very powerful technique to visualize and quantify soil macropore networks (e.g. Luo et al. 2010; Hu et al. 2015; Katuwal et al. 2015; Hu et al. 2016).

However, using XRCT, these studies mostly concentrated on agricultural (e.g. Mooney 2002; Pagenkemper et al. 2015; Bottinelli et al. 2016) and grassland soils (e.g. Bastardie et al. 2005; Martínez et al. 2010; Hu et al. 2015). For instance, Luo et al.

(2010) visualized the 3D morphology of macropore networks in two types of undisturbed soil columns that were taken from cropland and pasture, and quantified macropore characteristics, including macroporosity, macropore network density, total surface area, macropore size distribution, length density, length distribution, node density, mean hydraulic radius, tortuosity, inclination, and connectivity. Four repacked soil cores collected in SE France were incubated with two kinds of earthworms (*A. nocturna* versus *A. chlorotica*). After six weeks, Capowiez et al. (2011) reconstructed and quantified the 3D geometry of earthworm burrow, including macroporosity, burrow length, median burrow diameter, vertical deviation, branching rate, the number of burrows, and then assessed the impacts of earthworm species on burrow characteristics. However, to date, as far as we known, detailed studies on the 3D geometry of macropores in undisturbed soil columns that were extracted from forest slopes are rare. Only Auclerc et al. (2013) investigated the earthworm burrow structural features (mean diameter, burrow number, burrow distribution by soil depth) of two species (*Lumbricus terrestris* vs. *Aporrectodea caliginosa*) in repacked soil columns from an acidic forest of the Vosges Mountains, NE France by using XRCT. In addition, several researchers concluded that land use is among the main factor influencing macropore characteristics (Zhou et al. 2008; Mooney and Morris 2008; Luo et al. 2010). As a consequence, quantification of 3D macropores in forest soils is essential.

In Yunnan, Sichuan and Guizhou Province, China, extreme intense rainfall often trigger regional group landslides and debris flows in mountainous vegetated areas, which cause great losses of people's lives and properties (Xu and Huang 2011). For instance, Touzhai valley (Yunnan, China) is one of the extreme susceptibility area of geological hazard (Yunnan Institute of Geological Environment Monitoring 2003; Zhang et al. 2016). The intense rainfall-triggered potentially unstable slopes were threatening the villages at the downstream of this valley. Consequently, using XRCT, the objectives of this study are to (1) visualize the 3D macropore networks in undisturbed soil columns taken from a forest hillslope in Touzhai valley and (2) quantify the characteristics of 3D macropores including

macropore density, equivalent circular diameter (ECD), circularity, macroporosity, macropore volume distribution, macropore wall area density, branch density, node density, macropore length, tortuosity, inclination (angle), and hydraulic radius. Furthermore, in order to better describe the 3D macropores in Touzhai valley, we compared them with those in agricultural (Luo et al. 2010; Katuwal et al. 2015) and grassland soils (Luo et al. 2010).

1   Materials and Methods

1.1 Study site

The study site (27°34′N, 103°51′E) is located in Touzhai valley, approximately 30 km north-northeast of Zhaotong city (Yunnan province, Southwest China) and located at an elevation of 2250-2500 m above mean sea level (masl) (Figure 1). This region has a typical warm and humid plateau monsoon climate with a mean annual rainfall of 1082.7 mm and an annual mean temperature of 12.1°C and an annual mean relative humidity of 89% (35-year period from 1981 to 2015, data were derived from National Meteorological Information Center, China Meteorological Administration). The minimum, maximum and mean monthly precipitation are 38.8 mm (December), 185.9 mm (July) and 90.2 mm, respectively. The monthly precipitation has an unimodal distribution (Figure 2).

The vegetation at the site is a natural forest dominated by *Rhododendron decorum Fr.*, *Cyclobalanopsis glaucoides Schott.*, and *Yushania Keng f.* (Figure 1). The vegetation cover is nearly full at the site. Throughout the valley, residual soil depth ranges from 40 cm to 120 cm underlain by Permian Emeishan basalt ($P_2\beta$). The soil physical properties are presented in section 1.5 (see below). The soil type is classified as Histosols according to the USDA Soil Taxonomy. The soils is

a low acid soils with a pH between 4.7 and 5.5 and the dominating clay mineral is montmorillonite (Ren 2014). *Rhododendron decorum Fr.* belongs to evergreen broad-leaved forest (shrub) and is a shallow rooted plant. *Cyclobalanopsis glaucoides Schott.* is one of evergreen broad-leaved forest (tree) and the root morphology is heartroot (Zhou et al. 2001). The root of Yushania Keng f. is fibrous root system. These plants prefer low acid to neutral soils. Furthermore, the main soil animal is earthworm (*Pheretima tschiliensis*). *Pheretima tschiliensis* belongs to Pheretima species, Megascolecidae, also known as deep-burrowing earthworm. *Pheretima tschiliensis* prefers low acid to neutral and moist organic soils and creates permanent vertical continuous burrows. However, the density of earthworm is low (about 4 to 5 individuals m^{-2}). Details and additional information on valley characteristics and geological conditions can be found in Chen and Kong (1991) and Xu et al. (2007).
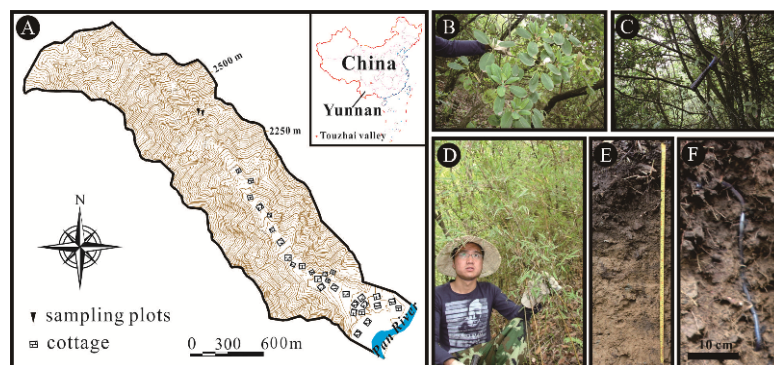

Figure 1 (A) Study site (Touzhai valley) and sampling plots; (B) *Rhododendron decorum Fr.*; (C) *Cyclobalanopsis glaucoides Schott.*; (D) *Yushania Keng f.*; (E) Typic soil profile: the soil is Histosols according to the USDA Soil Taxonomy; (F) Earthworm (*Pheretima tschiliensis*).
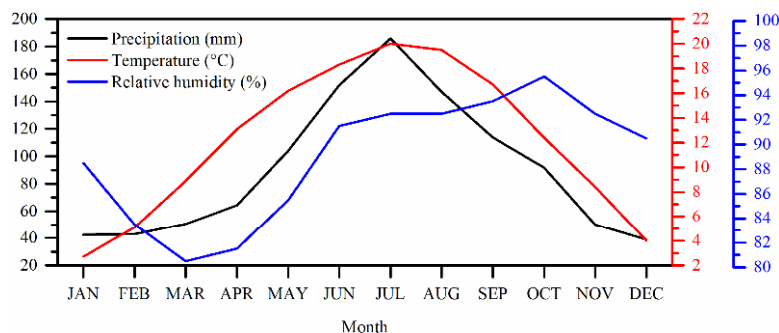

Figure 2 Monthly distribution of precipitation, temperature and relative humidity for study site (35-year period from 1981 to 2015). Date source: National Meteorological Information Center, China Meteorological Administration.

1.2 Soil sampling

Two undisturbed soil columns (hereafter denoted as S1 and S2) of 250 mm in length, 250 mm in width and 500 mm in height were taken from two sampling plots in April 2013 from about 6 to 56 cm depth because the soil structure of the top 6 cm soil layer was very weak and then prone to disturbance. The two sampling plots at a gentle slope with a slope of 15%, and the distance between the two plots were approximately 5 m. The soil depth of two plots was about 80 cm.

Polyvinyl chloride cylinders are often used to extract undisturbed soil cores from agricultural (such as Mooney 2002; Pagenkemper et al. 2015) and grassland soils (such as Bastardie et al. 2005; Hu et al. 2015). However, it is not total precise for forest soils due to the existence of stones and roots. Therefore, at this study site, the excavation procedure for each undisturbed soil core was as follows (Figure 3): (1) the aboveground vegetation was carefully clipped to ground level with minimum disturbance, and litter was completely removed to expose bare soil; (2) a large pit (100 cm length×100 cm width×60 cm depth) was dug in the field using a pick, keeping the reserved central clod of the pit undisturbed; (3) the soil clod was carved carefully with small shovels and hand tools, the stones around the soil clod were removed and roots were cut with pliers; (4) four vertical lateral sides and the top surface of the soil column were prepared carefully with a knife and cleaned with a brush to remove loose soil particles resulting from digging; (5) the soil column was sealed with plastic film and wrapped with cloth and subsequently four wooden blocks with 250 mm width, 500 mm length and 10 mm thickness were used to house the soil column; (6) the soil column was trimmed at the bottom, the bottom of soil column was sealed with plastic film and cloth, the both ends of soil column were sealed with two wooden blocks with 250 mm width, 250 mm length and 10 mm thickness. Finally, soil column was tighten with iron wire, and then transported carefully to avoid any compaction and evaporation to the lab for CT scanning.

1.3 X-ray computed tomography scanning

Both soil columns, at in-situ soil water content conditions, were scanned with a medical scanner, Somatom Sensation Open 40 (Siemens AG, Erlangen, Germany) at the Radiodiagnosis Center, The Third People's Hospital of Yunnan Province. Each soil column was placed horizontally on the bench so that the x-ray intersected the soil column perpendicular to its longitudinal axis. Then, spiral scanning performed using a voltage of 120 kV, a current of 176 mA, a scan speed of tow rotations/s, and a slice thickness of 1.5 mm without intervals between two successive slices. Each soil column was generated 334 images with 512×512 pixels per slice for the field of view of 484×484 mm, thus producing voxels with a resolution of $0.945 \times 0.945 \times 1.5$ mm in the reconstructed image. The images were 16-bit (DICOM format) in which the voxel values represented the liner attenuation coefficient in Hounsfield units (Capowiez et al. 2011; Katuwal et al. 2015) and were used to further process.

Figure 3 The sampling procedure for each undisturbed soil core. (a) a pit was dug and the central clod was reserved; (b) four vertical lateral sides and the top surface of the soil column were well prepared, the length of rule is 50 cm; (c) the soil column was wrapped with plastic film, cloth and wooden blocks; (d) soil column was tighten with iron wire.

1.4 Image processing

1.4.1 Pre-processing

Figure 4 shows the overall procedures of image processing followed in this study. All images were manipulated using public domain software program ImageJ, version 1.51c (National Institutes of Health, USA) and VolView 3.4 computer software (Kitware Inc, USA). First, a grayscale image stack was reconstructed based on these slices. And then, the image stack was cropped to a region of interest (ROI) of 200 mm in width, 200 mm in length from near the center of images, and 25 mm of the soil at both ends of each column were cropped to avoid artifacts due to the uneven surfaces of the soil samples. As a result, soil columns 200 mm in width, 200 mm in length and 450 mm in height (212×212×300 pixels) were used for following analysis. The soil columns are hereafter referred to as object soil columns (S1 and S2). Consequently, the object soil columns are representative of the depths 85 to 535 mm in the soil profile.
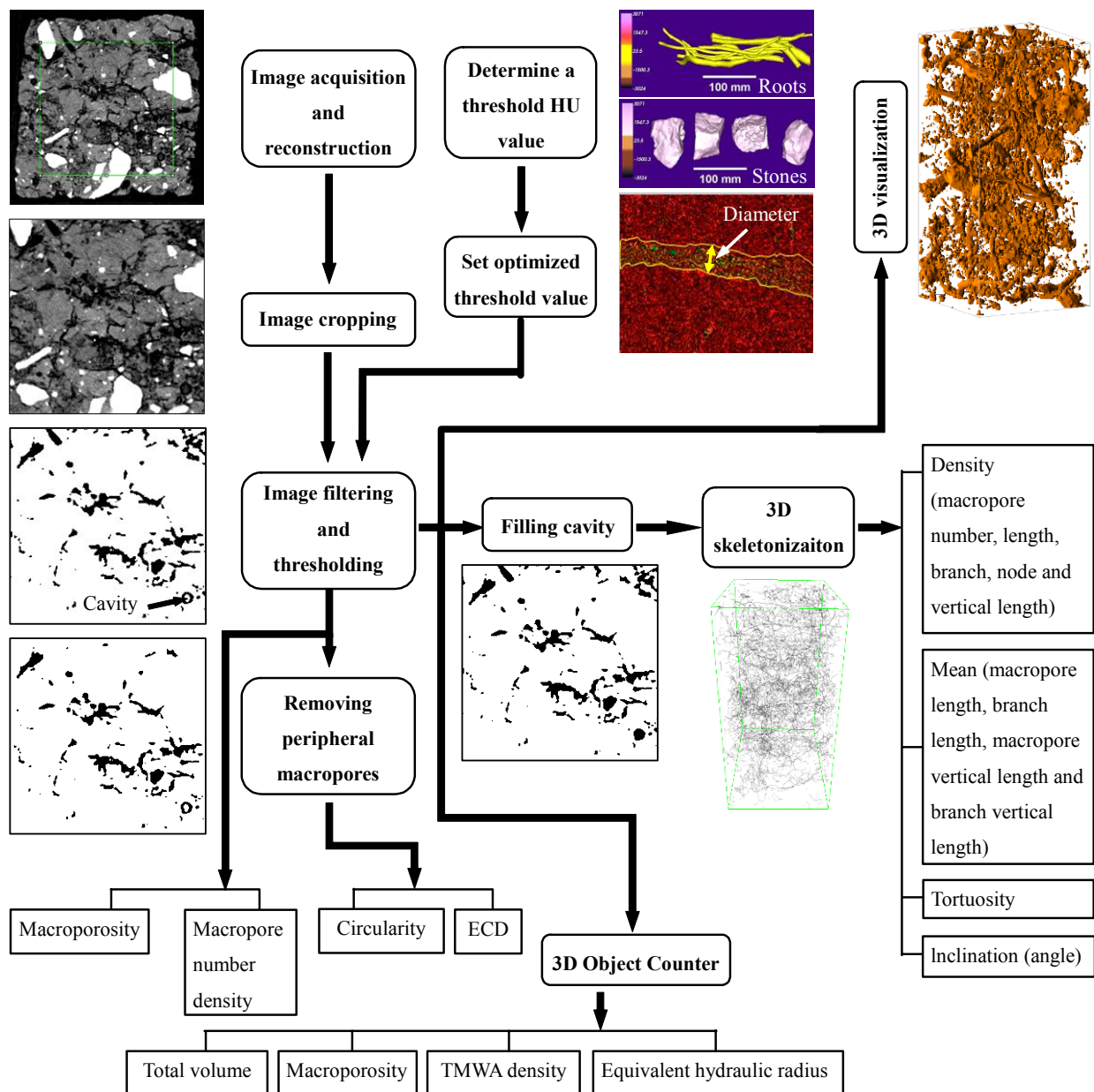
After that, a 3D median filter with a

Figure 4 The procedures used in present study for image processing and quantification of macropore networks.

neighborhood of two pixels was used to reduce the noise in the image stack (Luo et al. 2010). Hounsfield Units (HU) is linearly related to the bulk density of the soil (Schrader et al. 2007; Perret et al. 1999). Therefore, HU was often used to segment macropores (Langmaac et al. 1999; Katuwal et al. 2015; Rogasik et al. 2014). HU thresholding scheme as described by Hou (2015) was applied in this study. Briefly described, first, fresh roots and stones in soils were scanned with a medical scanner, the HU ranges of fresh roots and stones were determined using VolView 3.4 computer software. For instance, in our case, the HU range was −594~248 HU for the roots and 1379~3071 HU for the stones, respectively (Figure 4). Second, soil core with a known diameter of macropores was scanned by the CT scanner, the minimum value of these ranges, namely, −594 HU, was used as the threshold value to calculate the macropore size based on image analysis using ImageJ 1.51c, and then compared it with the authentic size. If the difference between them was too large, another threshold value was selected until the difference was less than 1%. A value of −594 HU was selected as the threshold value in this study. The grayscale image stack was translated into binary images stack, the black areas indicated macropores and the white areas indicated dense areas.

After segmentation, all macropores which touched the perimeter of the ROI (hereafter denoted as peripheral macropores) were eliminated since these macropores may be cut by the image boundary and their morphology not presented perfectly in the binary images. In this study, pores ≥ 1.066 mm in diameter were referred to as macropores.

1.4.2 Visualization and quantification of macropore networks

The variations in macroporosity, macropore number density, circularity and Equivalent Circular Diameter (ECD) with soil depth were analyzed by calculating these values for each slice (1.5 mm thickness) of the binary image of each object soil column. Exclusion of the peripheral macropores resulted in a reduction in macroporosity values for the soil columns by 27% to 33%. The difference in the two macroporosity with and without peripheral macropores was large. Therefore, only the circularity and ECD of each macropore were

computed based on the binary image without peripheral macropores. Macroporosity ($m^3\ m^{-3}$) is the ratio of the total volume of all macropores to the volume of the ROI. Macropore number density (number m^{-2}) is the ratio of the number of macropores to the area of the ROI. The circularity and ECD of macropores were calculated based on the surface area of the macropore and its perimeter according to the following equations: circularity=4π (area/perimeter^2), ECD=2(area/π)$^{0.5}$. These values were obtained using the Analyze Particles plugin in ImageJ.

Macropore networks were visualized using the Volume Viewer plugin in ImageJ. The skeletons of macropore networks were generated using the Skeletonize 3D plugin (Doube et al. 2010). The skeleton of a macropore is its central line with a thickness of one voxel. We observed a few circular macropores in binary images, i.e., a few cavities in the object (Figure 2). Because this plugin runs based on a classical 3D thinning algorithm (Lee et al. 1994). Thus, these cavities must be filled using the Analyze Particles plugin prior to skeletonization of the macropores. If not, this method could overestimate the macropore length.

After that, macropore density, macropore length density, branch density, macropore node density, mean macropore length, mean branch length, mean tortuosity, macropore vertical length
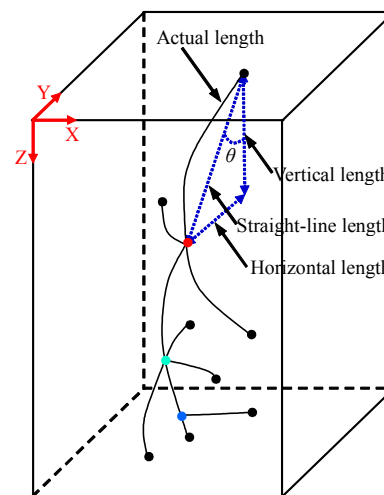

Figure 5 A macropore skeleton network with ten branches and three nodes in a soil column. Black segment is branch. Black dot is end point, but it isn't node. Blue dot, purple dot and red dot is junctions point, triple point and quadruple point, respectively and they are nodes. The actual length, straight-line length, vertical length, horizontal length and inclination of a branch are shown in this schematic diagram.

density, mean macropore vertical length, mean branch vertical length and mean angle for each object soil column were derived from 3D skeletons of the macropores using the Analyze Skeleton plugin (Doube et al. 2010). A macropore is a 3D network that is a set of branches that are interconnected by nodes (Figure 5). These terminologies have been detailedly introduced by Katuwal et al. (2015) and Luo et al. (2010), and are resumed in Table 1. The vertical length of a macropore branch represents the vertical continuity and is important to gravity flow (Luo et al. 2010). The inclination of a macropore branch was characterized by an angle (°) away from vertical direction (Figure 5). Thus, the smaller this angle, the more vertical the macropore network. Finally, 3D skeletons of the macropore networks were visualized using the 3D Viewer plugin (Schmid et al. 2010).

From the 3D binary image, the total volume and total macropore wall area (TMWA) of macropore networks systems were obtained using the 3D Object Counter plugin (Bolte and Cordelieres 2006) in ImageJ. Then, the overall macroporosity, TMWA density and mean equivalent hydraulic radius were calculated. Three terminologies are also summarized in Table 1.

1.5 Basic soil physical properties

After CT scanning, each column was divided into five soil layers at 10 cm depth intervals. For each soil layer, first, three undisturbed soil cores (5 cm in diameter, 5 cm in height) were taken and then oven-dried at 80°C (for soils with organic matter content >10%) or 105°C (for soils with organic matter content ≤10%) to a constant weight to determine the soil bulk density (Nanjing Hydraulic Research Institute 1999). Afterwards, the remaining soils was oven dried (80°C or 105°C-48 h), crushed and sieved to determine particle size distribution and organic matter content. The fraction of particles with a diameter of >0.075 mm was determined by wet sieving. The particle size (diameter<0.075 mm) analysis was performed using pipette method, where the rate of descent of the soil particles is used as a proxy for particle size (Sohrt et al. 2014). Organic matter content was determined by the potassium dichromate volumetric method (Zhou et al. 2009). Next, gravel (particle size > 2 mm) volume and weight was measured by water displacement in a graduated cylinder and by electronic balance, respectively. Then, the particle density of gravel was calculated. In addition, the particle density of fine grained soil

Table 1 Various terminologies of 3D macropore network

Terminology	Definition	Unit
Macropore density	The number of macropores in a unit volume	number m^{-3}
Macropore length density	The total actual length of macropores in a unit volume	km m^{-3}
Macropore branch density	The total number of all branches in a unit volume	number m^{-3}
Macropore node density	The number of nodes (intersections where at least two macropore branches connect) in a unit volume	number m^{-3}
The mean macropore length	The ratio of the total actual lengths of all macropores to the number of macropores	mm
The mean branch length	The ratio of the total actual lengths of all branches to the number of branches	mm
The mean tortuosity	The ratio of the total actual macropore length to the total straight-line distance of all the macropores	-
Macropore vertical length density	The total vertical length of all macropore branches in a unit volume	km m^{-3}
The mean macropore vertical length	The ratio of the total vertial lengths of all macropores to the number of macropores	mm
The mean branch vertical length	The ratio of the total vertical lengths of all branches to the number of branches	mm
The angle of a branch	It was calculated as: θ = arccos (vertical length/straight-line length)	°
The overall macroporosity	The ratio of the total volume of all macropores to the volume of object soil column	m^3 m^{-3}
The TMWA density	The total macropore wall area (TMWA) in a unit volume	m^2 m^{-3}
Mean equivalent hydraulic radius	Assuming that all macropores are cylindrical, it was computed by the total volume and total actual length of the all macropores. i.e., r=[total volume/(total actual length×π)]$^{0.5}$	mm

(particle size ≤ 2 mm) was determined by pycnometer method. Finally, porosity of the soil columns was calculated from bulk density, particle densities for fine grained soils and for gravels (Legout et al. 2009). Measured results of the soil physical properties are summarized in Table 2.

As shown in Table 2, organic matter decreased (varied from 16.69% to 2.09%) with depth (at a range of 60-560 mm). The soils have a high porosity (between 76.16% and 87.37%), a low bulk density (between 0.281 and 0.588 g. cm^{-3}) and a high gravel content (between 26.97 and 42.76%). Furthermore, the topsoil have a high organic matter (>7%).

1.6 Compared studies

Before illustrating the 3D geometry and topology of macroporess in the forest soils, it is important to mention that, up to now, there is little or no consensus for the definition of macropores (Noguchi et al. 1997; Feyen et al. 1998; Perret et al. 1999; Pierret et al. 2002; Buczko et al. 2006; Allaire et al. 2009). Macropores have been defined differently by various investigators or it is not defined at al (Noguchi et al. 1997; Zhang et al. 2012). A large number of the definitions of a macropore based on the ECD in soil literature were summaried by Beven and Germann (1982), Perret et al. (1999), and Zhang et al. (2012). They found that the lowest boundary of macropores varied from 30 to 10 000 μm and these definitions are conflicting. This is in part because different types of macropore have distinct geometries and in part because of the difference in resolution of CT scanner (Noguchi et al. 1997; Allaire et al. 2009). Therefore, it is more or less impossible to directly compare and discuss macropore characteristics between different investigators (Noguchi et al. 1997; Sheng et al. 2016).

However, in this study, the definition proposed by Luxmoore et al. (1990) was followed. They considered that macropore includes all pores with ECD ≥1 mm. In present study, pores ≥ 1.066 mm in diameter, were referred to as macropores. Consequently, the present study was only compared with Luo et al. (2010) and Katuwal et al. (2015) studies because the lowest boundary of macropores are comparable (0.75 mm for Luo et al. (2010), 1.2 mm for Katuwal et al. (2015)) and more detailed 3D macropore characteristics in agricultural and grassland soils were reported by Luo et al. (2010) and Katuwal et al. (2015).

The studied site of Luo et al. (2010) was located in the Ridge and Valley Physiographic Region of Pennsylvania. Cropland sites had conventional tillage and rotation cropping of corn (*Zea mays* L.) and soybean (*Glycine max* (L.) *Merr.*). Pasture sites were grazed by animals (cows and horses). The soil series are Hagerstown silt loam (Typic Hapludalfs) and Morrison sand (Ultic Hapludalfs). The parent material is limestone and sandstone, respectively. In cropland sites, Hagerstown silt loam soils have a high silt content (52%–68%) and a low rock fragment (>2 mm in size) content (<2%). Morrison sand soils have a high sand content (84%–88%), a high rock fragment content (20%–25%), a low organic matter content (<2%). However, in pasture sites, Morrison sand soils have a low rock fragment content (<5%). Six undisturbed soil columns (four for Hagerstown silt loam and two for Morrison sand, 102 mm in diameter and 350 mm in length) were randomly sampled from cropland sites and pasture sites in

Table 2 Soil physical properties at the Touzhai valley

Soil column	Depth (mm)	Organic matter [a] (%)	Porosity (%)	Bulk density (g cm^{-3})	Sand [b] (%)	Silt [b] (%)	Clay [b] (%)	Gravel [b] (%)
S1	60-160	12.82	85.93	0.298	48.85	39.67	11.48	30.15
	160-260	7.09	80.05	0.447	41.50	48.00	10.50	28.69
	260-360	4.62	83.18	0.430	40.44	47.19	12.37	30.02
	360-460	3.96	78.79	0.519	37.52	48.47	14.01	35.71
	460-560	2.68	76.16	0.588	32.24	47.28	20.48	43.76
S2	60-160	16.96	87.37	0.281	47.40	39.89	12.71	29.75
	160-260	8.16	78.77	0.432	42.12	46.71	11.17	28.26
	260-360	4.32	81.54	0.412	39.55	47.72	12.73	26.97
	360-460	2.60	78.53	0.502	38.14	45.55	16.31	31.46
	460-560	2.09	76.96	0.533	33.95	46.20	19.85	28.51

Notes: Textural classification was according to the USDA soil taxonomy; [a] Measured by potassium dichromate volumetric method; [b] Clay <0.002 mm, silt 0.002-0.05 mm, sand 0.05-2 mm, gravel ≥2 mm; percentage by weight.

July 2007, respectively.

The studied site of Katuwal et al. (2015) was located in Silstrup (56°55′56″ N, 8° 38′44″ E), in the northwestern part of Jutland, Denmark. The field was cultivated with barley, fodder beet and red fescue (Norgaard et al. 2013). According to the USDA soil classification system, the soil types are classified as Alfic Argiudoll and Typic Hapludoll (Norgaard et al. 2013). The soil texture is characterized by sandy loam and loam with high sand content (52.8%), low organic carbon (2%) and low porosity (44%). Seventeen undisturbed soil samples (19 cm diameter and 20 cm in height) were sampled from the topsoil in October 2010.

1.7 Statistical analysis

Non-parametric Wilcoxon signed rank tests were performed to test significance of difference between global macropore characteristics for different soils (the forest soil vs. the agricultural soils and the grassland soils). In the forest soils, the relation between the density of macropores and the macroporosity was measured by linear regression and calculation of the Pearson correlation coefficient (R_{S1} for S1, R_{S2} for S2). All statistical analyses were conducted in Statistical Package for the Social Sciences statistical analysis software (Version 17.0) with level of significance at $P<0.05$.

2 Results

2.1 Visualization of macropore networks

3D visualization of macropore networks in the two soil columns are shown in Figure 6 and different types of macropores could be identified. Previously, we had carried out five dye tracer experiments in the field (i.e., 1 m² surface area) in this study site and found a few earthworm burrows in the forest soils. However, earthworm burrow was did not observed in the two soil columns due to the density of earthworm was low, namely, about 4 to 5 individuals m⁻². Thus, the highly continuous, relatively large, round in shape and tubular macropore in these forest soil columns may be root channels (Luo et al. 2010). They constituted an important proportion of the macropore networks in the two soil columns. Moreover, because we had observed in situ that organic matter has downward migrated through the root channels during the sampling, the irregular, smaller and less continuously distributed macropores were likely inter-aggregate macropores (the voids between aggregates) (Luo et al. 2010) and other macropores without knowing origin (Figure 6c). In addition, a few circular macropores could be observed in binary images (Figure 4). These macropores may be associated with root-soil interface because the rhizosphere was stained by dyes in dye tracer experiments in situ.

(a) S1-macropore networks   (b) S2-macropore networks   (c) macropores without knowing origin
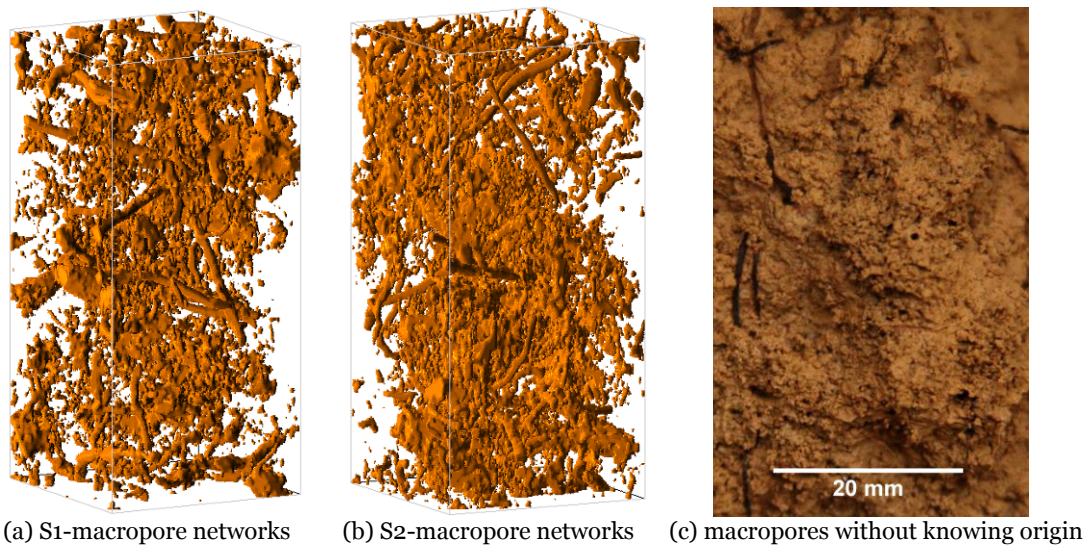
Figure 6 3D visualization of macropore networks ((a), (b)) for the object soil columns of S1 and S2 and macropores without knowing origin ((c)). This kind of macropores ((c)) was very common in the forest soils in present study sites but the formation mechanism of these macropores was not clear and needs further study.

Compared with the agricultural soils (see Figure 4 in Katuwal et al. 2015; Figures 3 and 4 in Luo et al. 2010) and the grassland soils (Figures 3 and 4 in Luo et al. 2010), macropore networks in the forest soils tend to be more complex. First, root channels in the forest soils were larger, deeper and longer. Furthermore, in the forest soils, the vertically oriented macropores were less. Additionally, the large number of the irregular macropores in the forest soils.

2.2 The variation of macropore number density, macroporosity, ECD and circularity with soil depth

The distributions of macropore number density, macroporosity, average ECD and average circularity with depth in the soil profile for two object soil columns (S1 and S2) are presented in Figure 7. In comparison, the variation of these characteristics with depth was significantly larger in the forest soils (Figure 7) than in the agricultural soils (Figures 5 and 6 in Katuwal et al. 2015; Figure 5 in Luo et al. 2010) and the grassland soils (Figure 5 in Luo et al. 2010). Further, the distribution patterns differed significantly among the three kinds of soils with different land-use. The depths of macropore distributions were also significantly larger in the forest soils than in the agricultural soils and the grassland soils (Luo et al. 2010; Katuwal et al. 2015).

Macropore number density fluctuated around 1513 number m^{-2} at soil depths between 85 mm and 400 mm and increased at soil depths of 400–436 mm, peak was 2250 number m^{-2}, then declined at soil depths from 436 to 535 mm for S1 (Figure 7a). For S2 (Figure 7a), macropore number density increased in the 85–371 mm soil layer, peak was 2975 number m^{-2}, and decreased at soil depths of 371–535 mm. In contrast,

macropore number density always decreased with depth in the agricultural soils (Katuwal et al. 2015).

Macroporosity increased wavily with depth, especially at soil depths of 130– 270 mm, peak was 0.135 m^3 m^{-3}, and declined sharply at 270 mm soil depth, then slightly waving as soil depth increased at 390 mm soil depth for S1 (Figure 7b). Macroporosity increased at soil depths between 85 mm and 283 mm and declined at 283 mm soil depth, then increased dramatically at 452 mm soil depth, peak was 0.149 m^3 m^{-3} and then decreased sharply at 482 mm for S2 (Figure 7b). Nevertheless, Katuwal et al. (2015) reported that in most of the agricultural soil samples with macroporosity higher than 0.008 cm^3 cm^{-3} (i.e., 0.008 m^3 m^{-3}), macroporosity variation with depth was more uniform. For soil under the grass, macroporosity first decreased with depth and increased slowly,
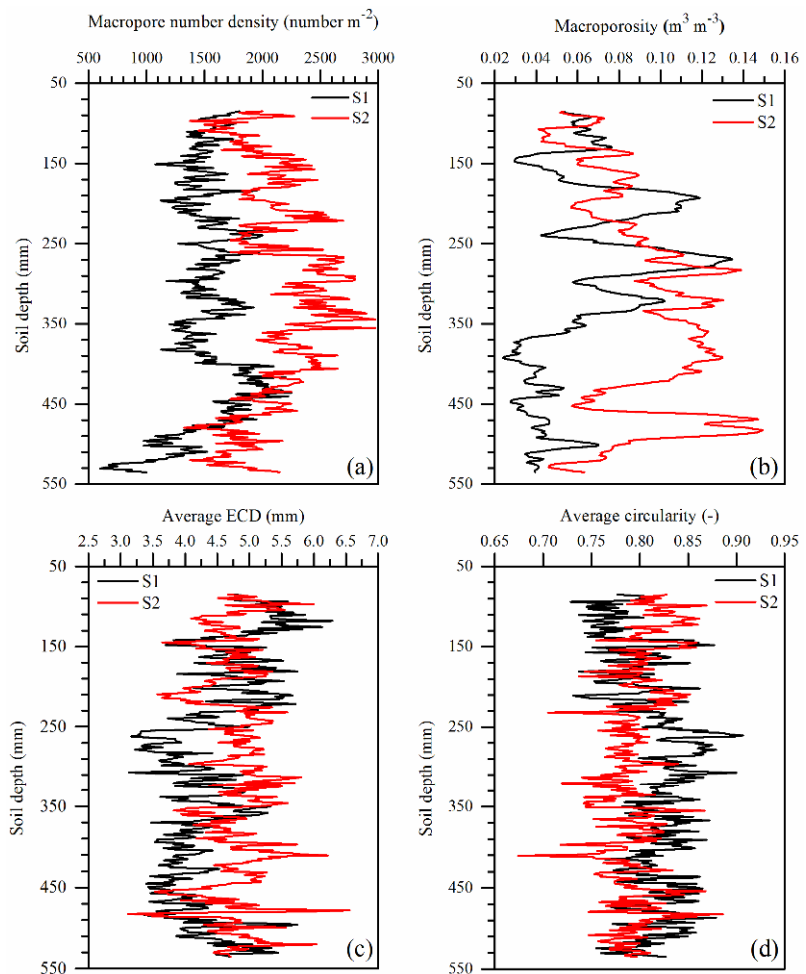

Figure 7 Macropore number density, macroporosity, average ECD and average circularity distribution along the soil depth (85 to 535 mm) for S1 and S2.

and then declined as soil depth increased (Luo et al. 2010).

Average ECD for each slice varied from 3.129 to 6.291 mm and varied from 3.114 to 6.556 mm for S1 and S2, respectively (Figure 7c). However, ECD at all depths ranged from 1.067 to 53.759 mm and ranged from 1.067 to 65.146 mm for S1 and S2, respectively. Average circularity for each slice was between 0.728 and 0.907 and between 0.674 and 0.886 for S1 and S2, respectively (Figure 7d).

2.3 Global macropore characteristics

2.3.1 Macropore density, macroporosity, macropore volume distribution and TMWA

The global macropore characteristics of the three kinds of soils are listed in Table 3. Macropore density was significantly less for the forest soils (ranged from 1.151 to 1.228×10^5 number m^{-3}, with an average of 1.190×10^5 number m^{-3}) than both the agricultural soils ($P<0.05$) and the grassland soils ($P<0.05$). Katuwal et al. (2015) reported that macropore density ranged from 0.70 to 3.69×10^5 number m^{-3} and with an average of 2.39×10^5 number m^{-3} in the agricultural soils. Macropore density in the cropland ranged between 6.61 to 8.47×10^5 number m^{-3}, with an average of 7.65×10^5 number m^{-3}, and in the grassland, the range was from 8.76 to 13.73×10^5 number m^{-3}, with an average of 11.54×10^5 number m^{-3} (Luo et al. 2010).

In contrast, soil macroporosity was greater in the forest soils (varied from 0.062 to 0.090 m^3 m^{-3}, with an average of 0.076 m^3 m^{-3}) than that in the agricultural soils ($P<0.05$) and the grassland soils ($P<0.05$). For agricultural soils, Luo et al. (2010) calculated that macroporosity was between 0.022 and 0.032 m^3 m^{-3}, with an average of 0.027 m^3 m^{-3}. Further, Katuwal et al. (2015) computed that the range was between 0.0038 and 0.0166 m^3 m^{-3}, with an average of 0.009 m^3 m^{-3}. In the grassland, soil macroporosity varied within a range of 0.031 to 0.074 m^3 m^{-3} with an average value of 0.051 m^3 m^{-3} (Luo et al. 2010).

The volume distribution of the macropores in each object soil column (S1 and S2) plotted against the cumulative volume percentage of macropores is shown in Figure 8. The forest soils had larger macropore volume (ranged from about 1.34 mm^3 to 331,213.469 mm^3, with an average of 482 mm^3 for S1, and the range was from 1.34 to 1,359,530 mm^3, with an average of 655 mm^3 for S2) as compared to the agricultural soils and the grassland soils. More than 90% of the macropore volume consisted of macropores with volume >1000 mm^3 for S1 and 93% for S2. The largest macropore with a volume of 331,213.469 mm^3 in S1 occupied about 30% of

Table 3 Global macropore characteristics of the forest soils (S1 and S2), agricultural soils (AS), and the grassland soils (GS)

Soil column	MD	BD	ND	MP	TMWA density	MALD	MVLD	MHR
	(×10^5) number m^{-3}			m^3 m^{-3}	m^2 m^{-3}	km m^{-3}		mm
S1	1.151	2.934	1.927	0.062	55.818	2.630	1.214	2.738
S2	1.228	5.074	3.884	0.090	90.532	4.663	2.204	2.486
Mean	1.190	4.004	2.906	0.076	73.175	3.647	1.709	2.612
AS1 [a]	2.39	4.38	1.21	0.009	15.88	2.42	—	—
AS2 [b]	7.65	—	2.62	0.027	26.83	4.94	1.299	0.71
GS [b]	11.54	—	4.44	0.051	47.94	9.46	2.397	0.73
Soil column	MMAL	MMVL	MBAL	MBVL	MT	MA	MHR
	mm				-	°	mm
S1	22.856	10.550	8.967	4.139	1.279	51.692	2.738
S2	37.962	17.947	9.189	4.344	1.277	50.708	2.486
Mean	30.409	14.248	9.078	4.242	1.278	51.200	2.612
AS1 [a]	10.11	—	5.48	—	1.25	—	—
AS2 [b]	—	—	—	—	1.63	42.367	0.71
GS [b]	—	—	—	—	1.71	37.733	0.73

Notes: MD: macropore density, BD: branch density, ND: node density, MP: macroporosity, TMWA density: total macropore wall area density, MALD: macropore actual length density, MVLD: macropore vertical length density, MMAL: mean macropore actual length, MMVL: mean macropore vertical length, MBAL: mean branch actual length, MBVL: mean branch vertical length, MT: mean tortuosity, MA: mean angle, MHR: mean hydraulic radius. —: no data.
[a] The mean of seventeen soil samples that taken from an agricultural field in Silstrup, Denmark. The lowest boundary of macropores was 1.2 mm in diameter. Detailed data see Table 2 in Katuwal et al. (2015).
[b] The mean of six soil samples that collected from two cropland sites and two pasture sites, respectively, in Pennsylvania, USA. The lowest boundary of macropores was 0.75 mm in diameter. Detailed data see Table 2 in Luo et al. (2010).

the total macropore volume, in S2, the largest macropore with a volume of 1,359,530 mm³ occupied about 83% of the total macropore volume. However, Luo et al. (2010) reported that the mean macropore volume was 35 mm³ and 46.4 mm³ for the agricultural soils and the grassland soils, respectively. The proportion of macropores with volume >1000 mm³ ranged from 45.19% to 67.61% for the agricultural soils, and in the grassland soils, the ranges was from 44.83% to 77.19% (Luo et al. 2010).

In agreement with the macropore volumes, the total macropore wall area density was quite higher for the forest soils than that for the agricultural soils ($P<0.05$) and the grassland soils ($P<0.05$). The TMWA density in the forest soils ranged from 55.818 to 90.532 m² m⁻³ (Table 3), however, the ranges was between 5.23 and 26.90 m² m⁻³ in the agricultural soils (Katuwal et al. 2015). The TMWA density ranged between 23.59 to 31.11 m² m⁻³ and between 27.30 to 60.90 m² m⁻³ in the soils under the crop and the soils under the pasture, respectively (Luo et al. 2010).

2.3.2 Macropore branch, node and macropore length

Macropore branch, node, and macropore length density were calculated based on the skeletons of macropores (Figure 9). Macropore branch density of the forest soils was smaller than that of the agricultural soils, but the difference was not statistically significant ($P>0.05$). Macropore node density of the forest soils was greater than that of the agricultural soils, but smaller as compared to the grassland soils, but these differences

were not statistically significant ($P>0.05$). Macropore branch density ranged from 2.934 to $5.074×10^5$ number m⁻³ and the node density ranged between 1.927 to $3.884×10^5$ number m⁻³ for the forest soils. Whereas, for the agricultural soils, Katuwal et al. (2015) reported that macropore branch density ranged from 1.29 to $7.02×10^5$ number m⁻³ and macropore node density ranged from 0.38 to $2.38×10^5$ number m⁻³. Macropore node density for the agricultural soils and the
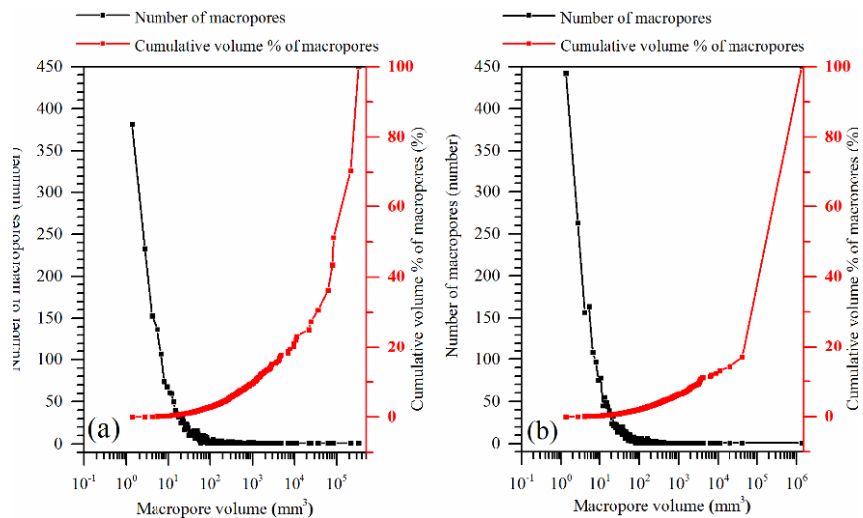

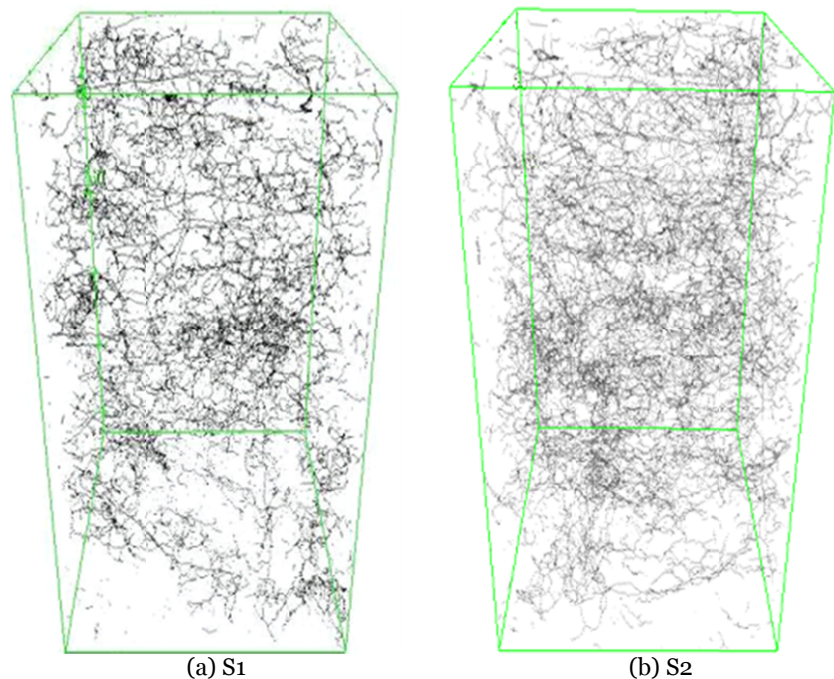**Figure 8** Macropore volume distributions of the two forest soil columns (a-S1, b-S2).

Figure 9 3D skeletons of macropore networks in the soil columns of forest soils.

grassland soils varied from 1.87 to 3.05×10⁵ number m⁻³ and from 2.39 to 5.85×10⁵ number m⁻³, respectively (Luo et al. 2010).

Overall, macropore length density for the forest soils was comparable with that for the agricultural soils ($P>0.05$), but smaller as compared to the grassland soils ($P<0.05$). For the forest soils, macropore actual length density and vertical length density ranged from 2.630 to 4.663 km m⁻³ and from 1.214 to 2.204 km m⁻³, respectively. For the agricultural soils, Katuwal et al. (2015) computed that macropore actual length density was between 0.71 and 3.91 km m⁻³. Macropore actual length density and vertical length density ranged from 4.47 to 6.10 km m⁻³ and from 0.54 to 1.95 km m⁻³, respectively, in the agricultural soils (estimated based on the Figure 8 in Luo et al. 2010). However, for the grassland soils, macropore actual length density ranged from about 4.50 to 12.93 km m⁻³ and the macropore vertical length density ranged from about 1.07 to 3.17 km m⁻³ (Luo et al. 2010).

In contrast, our results showed that the forest soils had greater mean macropore actual length, mean macropore vertical length, mean branch actual length, and mean branch vertical length than those the agricultural soils and the grassland soils. Mean macropore actual length and mean branch actual length was 30.409 mm and 9.078 mm, respectively, for the soils in forest, which were about 3.01 and 1.66 times higher than those in cropland ($P<0.05$) (Katuwal et al. 2015), respectively. In the forest soils, mean macropore vertical length and mean branch vertical length was 14.248 mm and 4.242 mm, respectively. As can be seen from the Table 3, mean macropore density was 7.65×10⁵ number m⁻³ and 11.5×10⁵ number m⁻³ for the agricultural soils and the grassland soils (Luo et al. 2010), respectively, which was about 6.43 and 9.70 times higher than that for the forest soils. However, mean macropore actual length density was 4.94 km m⁻³ and 9.46 km m⁻³ for the agricultural soils and the grassland soils (Luo et al. 2010), respectively, which only was 1.35 and 1.42 times higher than that for the forest soils. Mean macropore vertical length density was 1.299 km m⁻³ and 2.397 km m⁻³ for the agricultural soils and the grassland soils (estimated based on the Figure 8 in Luo et al. 2010), respectively, which only was 0.76 and 1.40 times the that in the forest soils. The above results demonstrate that the mean macropore actual length and mean macropore vertical length in the forest soils are larger than those in both the agricultural soils and the grassland soils.

2.3.3 Macropore tortuosity, angle and hydraulic radius

On the whole, the tortuosity of the forest soils (1.278 on average) was smaller relative to that of the agricultural soils (but not at a significant level ($P>0.05$)) and the grassland soils ($P<0.05$) (Table 3). This mean was comparable with that of Katuwal et al. (2015), who reported that the tortuosity of the agricultural soils varied within a close range of 1.23 to 1.28 with an average value of 1.25. Furthermore, Luo et al. (2010) calculated that the agricultural soils had the tortuosity of 1.46–1.91, while that for the grassland soils was 1.56–1.87.

The forest soils had a mean angle of 51.200° compared to 42.367° and 37.733° in the agricultural soils ($P>0.05$) and the grassland soils ($P<0.05$), respectively (Table 3). For the forest soils, mean hydraulic radius was 2.612 mm, which was about 3.68 and 3.58 times greater than that for the agricultural soil and the grassland soils, respectively ($P<0.05$) (Table 3).

3 Discussion

3.1 3 D morphology and spatial distribution of macropore networks

Results from this study demonstrated that macropore networks in the forest soils tend to be more complex and deeper as compared to the agricultural soils (Luo et al. 2010; Katuwal et al. 2015) and the grassland soils (Luo et al. 2010). The discrepancies may be attributed to the different types of macropores and different vegetation types for the different soils.

First, different types of macropores have distinct geometries (Luo et al. 2010; Hu et al. 2016) and the main types of macropores are different among the three kinds of soils. For instance, as can be seen from the Figure 6, root channels, inter-aggregate macropores and other macropores without knowing origin occur extensively in the forest soils. Furthermore, we had carried out five

dye tracer experiments in situ in this study site and found a large number of gravels (or stones) and roots were stained by dyes. The results suggested that stone-soil interface and root-soil interface are important macropores in the forest soils. These findings are consistent with those of Noguchi et al. (1997), Feyen et al. (1998), Laine-Kaulio et al. (2015), and Zhang et al. (2016). However, Luo et al. (2010) and Katuwal et al. (2015) reported that earthworm burrows and root channels constituted a significant proportion of the macropore networks in the agricultural soils and the grassland soils.

Second, different vegetation types have different types of root systems (Aubertin 1971; Pagenkemper et al. 2015). Thus, macropore networks that resulted from root systems have different morphology and spatial distribution. For example, *Rhododendron decorum Fr.*(shrub), *Cyclobalanopsis glaucoides Schott.* (tree), and *Yushania Keng f.* (grass). coexist in the study site. However, cropland sites (Luo et al. 2010) had rotation cropping of corn (*Zea mays* L.) and soybean (*Glycine max* (L.) *Merr.*). The field (Katuwal et al. 2015) was cultivated with barley, fodder beet and red fescue. Moreover, several researcher demonstrated that the root networks of woody vegetation such as forest and shrubland have greater depth, diameter, dispersion, and biomass than these of the root networks of herbaceous plants or cultivated crops (e.g. Lee and Lauenroth 1994; Jackson et al. 1996; Messing et al. 1997; Price et al. 2010).

Finally, as shown in Figures 7a, 7b, unlike the agricultural soils and the grassland soils, there were no significant positive correlations between the density of macropores and the macroporosity for the forest soils (R_{S1}=0.016, R_{S2}=0.317). This was because the ranges of macropore size were significantly larger in the forest soils than in the agricultural soils and the grassland soils. For example, Luo et al. (2010) reported that the maximum of volumetric macropores size was smaller than 100,000 mm³ for the agricultural soils and the grassland soils (Figure 6 in Luo et al. 2010). However, the maximum of volumetric macropores size was 331,213.469 mm³ and 1,359,530,mm³ for S1 and S2, respectively (Figure 8). Consequently, it is more appropriate to use macroporosity rather than the macropore number density to indicate the proportion of macropores in forest soils.

3.2 Global macropore characteristics

3.2.1 Macroporosity, macropore volume, TMWA, node density and hydraulic radius

The forest soils had higher macroporosity, larger macropore volume, higher TMWA density, higher node density, and larger hydraulic radius as compared to the agricultural soils and the grassland soils (Table 3). This finding suggests that the macropore networks in the forest soils have high inter-connectivity and can be explained by a combination of anthropogenic and natural factors. In summary, the well-developed macropore networks in the forest soils can be related to stable and high vegetation cover, low bulk density, high gravel content, high organic matter content, low silt content, and less anthropogenic disturbance (less soil compaction).

Vegetations have positive effects on the formation and development of macropore network. First, root systems play an important role in forming root channel and root-soil interface in forst soils (Noguchi et al. 1997; Price et al. 2010; Zhang et al. 2016). For instance, Noguchi et al. (1997) estimated that at Hitachi Ohta experimental watershed in Japan, about 55-70% of the macropores were formed by roots. Second, roots initiate aggregate formation, and root exudates and microbial activity stimulate production of humic cement, which enhances aggregate stability (Jirků et al. 2013). Thus, a large number of inter-aggregate macropores were observed in the forest soils. Third, plant canopy and litter cover protect macropores in topsoils against rain splash and wind-driven rain splash, reduce soil erosion, and maintain macropores and aggregate stability for long time (Hanson et al. 2004; Bodner et al. 2013; Marzen et al. 2015; Zhao et al. 2016; Prosdocimi et al. 2016; Rodrigo Comino et al. 2016a). Several researcher demonstrated that raindrop erosion destroys soil particles and aggregates, and subsequently transports fine soil particles, and thereby clogs macropores (Hanson et al. 2004; Lamandé et al. 2011; Bagarello et al. 2014; Marzen et al. 2015). In the forest site, the vegetation is long-term stable due to less anthropogenic disturbance. However, the cropland sites had rotation cropping and thereby most crops leave the soil surface unprotectd in a certain period of the

year (Luo et al. 2010). The pasture sites were grazed by animals: cows and horses (Luo et al. 2010). Therefore, soil erosion rates are much lower for the forest soils as compared to the agricultural and grassland soils. The results are in agreement with those reported by Auerswald et al. (2009); Cerdan et al. (2010); Rodrigo Comino et al. (2015).

Furthermore, mean bulk density (0.444 g cm⁻³) for the forest soils was less than one third of the mean bulk density for the agricultural soils (1.495 g cm⁻³) (Luo et al. 2010 and Katuwal et al. 2015) and the grassland soils (1.43 g cm⁻³) (Luo et al. 2010). Generally, the soils with lower bulk density often contains greater volume of macropores (Bottinelli et al. 2016).

Additionally, the greater rock fragment (or gravel, stone) content, the more temperate is the soil climate (Cerdà 2001). Therefore, rock fragment favorable for faunal activity and macropores formation (Cerdà 2001). For example, using scanning electron microscope, Certini et al. (2004) observed numerous hyphae and other living forms on the surface of the stones, in forest (silver fir (*Abies alba* Mill.) and European beech *(Fagus sylvatica* L.)) soils in Vallombrosa, Italy. Moreover, like as plant canopy and litter cover (already discussed above), surface rock fragment protect macropores against raindrop erosion (Cerdà 2001; Prosdocimi et al. 2016; Rodrigo Comino et al. 2016b). In addition, the forest soils have higher organic matter content as compared to the agricultural and grassland soils (Luo et al. 2010; Katuwal et al. 2015). Consequently, the forest soils more favorable for soil macropore development and stabilization (Hu et al. 2016; Prosdocimi et al. 2016; Zhang and Xu 2016).

On the contrary, in agricultural soils (Luo et al. 2010), the low macroporosity could be attributed to conventional tillage. Buczko et al. (2006) concluded that, the smaller numbers of macropores and lower connectitity of the macropore networks is found commonly in conventional tillage systems as compared with conservational tillage systems due to more disturbance of the topsoil. Furthermore, the low macroporesity in the grassland soils was likely associated with the compaction caused by grazing (Luo et al. 2010). Additionally, Hagerstown silt loam (agricultural and grassland soils, Luo et al. 2010) have higher silt content as compared to the forest soils (loam).

As a consequence, the Hagerstown silt loam was more susceptibility to raindrop impart, and not favorable for macropore development and stabilization (Hanson et al. 2004; Bagarello et al. 2014; Rodrigo Comino et al. 2016 a, b).

3.2.2 Macropore length, angle and tortuosity

Compared with the agricultural soils and the grassland soils (Luo et al. 2010; Katuwal et al. 2015), the forest soils had larger mean macropore length (including actual length and vertical length) and angle, and lower tortuosity (Table 3). These results suggest that macropore networks in the forest soils have high vertical continuity, less vertically oriented and high linearity.

The larger mean macropore length in the forest soils could be attributed to the amount of root systems was smaller but the total length of root systems was longer as compared to the agricultural soils and the grassland soils (Luo et al. 2010; Katuwal et al. 2015). Furthermore, in the forest soils, root channels and root-soil interfaces constituted an important proportion of the macropore networks. Therefore, the larger angle is mainly related to the root morphology. First, *Rhododendron decorum Fr. is* a shallow rooted plant, and the root morphology of *yclobalanopsis glaucoides Schott.* is heartroot (Zhou et al. 2001). They had a large number of lateral roots. Second, the shallow forest slope soils is underlay by solid bedrock, which favorable for root lateral growth (Luo 1984). In addition, generally speaking, the tortuosity of roots decreased with an increase of the diameter of roots. Therefore, the tortuosity of macropore network in the forest soils was low. Furthermore, more tortuous macropores in the agricultural and grassland soils may be due to the greater competition for food and space among more abundant earthworms in these soils (Luo et al. 2010).

4 Conclusions

The typical characteristics of 3D macropore networks in the forest soils as follow: (1) the main types of macropores are root channels, inter-aggregate voids, macropores without knowing origin, root-soil interface and stone-soil interface; (2) macropore networks tend to be more complex,

larger, deeper and longer; (3) the forest soils have high macroporosity, total macropore wall area density, node density, and large macropore volume, hydraulic radius, mean macropore length, angle, and low tortuosity; (4) the above results suggest that macropore networks in the forest soils have high inter-connectivity, vertical continuity, linearity and less vertically oriented.

However, unfortunately, the top 85 mm soil layer were not quantified in this study due to the soil structure was very weak and prone to disturbance during sampling. Consequently, an improved sampling method and a larger numbers of small scale soil samples (e.g., 90 mm diameter×90 mm length) extracted from the top soil layer are required for future 3D macropore characteristics studies. Furthermore, the temporal variability of macropore networks in the forest soils needs further investigation.

References

Alaoui A, Helbling A (2006) Evaluation of soil compaction using hydrodynamic water content variation: comparison between compacted and noncompacted soil. Geoderma 134(1): 97-108. DOI: 10.1016/j.geoderma.2005.08.016

Allaire SE, Roulier S, Cessna AJ (2009) Quantifying preferential flow in soils: A review of different techniques. Journal of Hydrology 378(1): 179-204. DOI: 10.1016/j.jhydrol.2009.08.013

Anderson E, Weiler M, Alila Y, et al. (2009) Dye staining and excavation of a lateral preferential flow network. Hydrology and Earth System Sciences 13(6): 935-944. DOI: 10.5194/hess-13-935-2009

Aubertin GM (1971) Nature and extent of macropores in forest soils and their influence on subsurface water movement. Res. Pap. NE-192. Upper Darby, PA: U.S. Department of Agriculture, Forest Service, Northeastern Forest Experiment Station.

Auclerc A, Capowiez Y, Guérold F, et al. (2013) Application of X-ray tomography to evaluate liming impact on earthworm burrowing activity in an acidic forest soil under laboratory conditions. Geoderma 202: 45-50. DOI: 10.1016/j. geoderma. 2013.03.011

Auerswald K, Fiener P, Dikau R (2009) Rates of sheet and rill erosion in Germany — A meta-analysis. Geomorphology 111(3): 182-193. DOI: 10.1016/j.geomorph.2009.04.018

Bagarello V, Castellini M, Di Prima S, et al. (2014) Soil hydraulic properties determined by infiltration experiments and different heights of water pouring. Geoderma 213: 492-501. DOI: 10.1016/j.geoderma.2013.08.032

Bastardie F, Capowiez Y, Cluzeau D (2005) 3D characterisation of earthworm burrow systems in natural soil cores collected from a 12-year-old pasture. Applied Soil Ecology 30(1): 34-46. DOI: 10.1016/j.geoderma.2013.03.011

Beven K, Germann P (1982) Macropores and water flow in soils. Water resources research 18(5): 1311-1325. DOI: 10.1029/WR018i005p01311

Bodner G, Scholl P, Loiskandl W, et al. (2013) Environmental and management influences on temporal variability of near saturated soil hydraulic properties. Geoderma 204: 120-129. DOI: 10.1016/j.geoderma.2013.04.015

Bogner C, Wolf B, Schlather M, et al. (2008) Analysing flow patterns from dye tracer experiments in a forest soil using extreme value statistics. European Journal of Soil Science 59(1): 103-113. DOI: 10.1111/j.1365-2389.2007.00974.x

Bolte S, Cordelieres FP (2006) A guided tour into subcellular colocalization analysis in light microscopy. Journal of microscopy 224(3): 213-232. DOI: 10.1111/j.1365-2818.2006.01706.x

Bottinelli N, Zhou H, Boivin P, et al. (2016) Macropores generated during shrinkage in two paddy soils using X-ray micro-computed tomography. Geoderma 265: 78-86. DOI: 10.1016/j.geoderma.2015.11.011

Buczko U, Bens O, Hüttl RF (2006) Tillage effects on hydraulic properties and macroporosity in silty and sandy soils. Soil Science Society of America Journal 70(6): 1998-2007. DOI: 10.2136/sssaj2006.0046

Capowiez Y, Pierret A, Daniel O, et al. (1998) 3D skeleton reconstructions of natural earthworm burrow systems using CAT scan images of soil cores. Biology and Fertility of Soils 27(1): 51-59. DOI:10.1007/ s003740050399

Capowiez Y, Sammartino S, Michel E (2011) Using X-ray tomography to quantify earthworm bioturbation non-destructively in repacked soil cores. Geoderma 162(1): 124-131. DOI:10.1016/j.geoderma.2011.01.011

Cerdà A (2001) Effects of rock fragment cover on soil infiltration, interrill runoff and erosion. European Journal of Soil Science 52(1): 59-68. DOI: 10.1046/j.1365-2389.2001.00354.x

Cerdan O, Govers G, Le Bissonnais Y, et al. (2010) Rates and spatial variations of soil erosion in Europe: A study based on erosion plot data. Geomorphology 122(1): 167-177. DOI: 10.1016/j.geomorph. 2010.06.011

Certini G, Campbell CD, Edwards AC (2004) Rock fragments in soil support a different microbial community from the fine earth. Soil Biology and Biochemistry 36(7): 1119-1128. DOI:

10.1016/j.soilbio.2004.02.022

Chen ZS, Kong JM (1991) A catastrophic landslide of sept.23,1991 at Touzhaigou of Zhaotong, Yunan province. Mountain Research 9(4): 265-268. DOI: 10.16089/j.cnki.1008-2786.1991.04.013 (In Chinese)

Doube M, Kłosowski MM, Arganda-Carreras I, et al. (2010) BoneJ: free and extensible bone image analysis in ImageJ. Bone 47 (6): 1076-1079. DOI: 10.1016/ j.bone.2010.08.023

Feyen J, Jacques D, Timmerman A, et al. (1998) Modelling water flow and solute transport in heterogeneous soils: A review of recent approaches. Journal of Agricultural Engineering Research 70(3): 231-256. DOI: 10.1006/jaer. 1998.0272

Hanson DL, Steenhuis TS, Walter MF, et al. (2004) Effects of soils degradation and managment practices on the surface water dynamics in the talgua river watershed in Honduras. Land Degradation & Development 15:367-381. DOI: 10.1002/ldr.603

Holden J (2009) Flow through macropores of different size classes in blanket peat. Journal of Hydrology 364(3): 342-348. DOI:10.1016/j.jhydrol.2008.11.010

Hu X, Li ZC, Li XY, et al. (2015) Influence of shrub encroachment on CT-measured soil macropore characteristics in the Inner Mongolia grassland of northern China. Soil and Tillage Research 150: 1-9. DOI:10.1016/j.still.2014.12.019

Hu X, Li ZC, Li XY, et al. (2016) Quantification of soil macropores under alpine vegetation using computed tomography in the Qinghai Lake Watershed, NE Qinghai–Tibet Plateau. Geoderma 264: 244-251. DOI:10.1016/ j.geoderma.2015.11.001

Huo RJ (2015) The study of macropore and permeability of wall vegetated slope soils based on CT scans. Master Thesis, Kunming University of Science and Technology, Kunming, Yunnan. p 26. (In Chinese)

Jackson RB, Canadell J, Ehlerlinger JR, et al. (1996) A global analysis of root distributions for terrestrial biomes. Oecologia 108 (3): 389-411. DOI: 10.1007/BF00333714

Jégou D, Capowiez Y, Cluzeau D (2001) Interactions between earthworm species in artificial soil cores assessed through the 3D reconstruction of the burrow systems. Geoderma 102(1): 123-137. DOI: 10.1016/S0016-7061(00)00107-5

Jirků V, Kodešová R, Nikodem A, et al.(2013) Temporal variability of structure and hydraulic properties of topsoil of three soil types. Geoderma 204: 43-58. DOI: 10.1016/j. geoderma.2013.03.024

Katuwal S, Norgaard T, Moldrup P, et al. (2015) Linking air and water transport in intact soils to macropore characteristics inferred from X-ray computed tomography. Geoderma 237: 9-20. DOI: 10.1016/ j.geoderma.2014.08.006

Laine-Kaulio H, Backnäs S, Koivusalo H, et al. (2015) Dye tracer visualization of flow patterns and pathways in glacial sandy till at a boreal forest hillslope. Geoderma 259: 23-34. DOI:10.1016/j.geoderma.2015.05.004

Lamandé M, Labouriau R, Holmstrup M, et al. (2011) Density of macropores as related to soil and earthworm community parameters in cultivated grasslands. Geoderma 162(3): 319-326. DOI: 10.1016/j.geoderma.2011. 03.004

Langmaack M, Schrader S, Rapp-Bernhardt U, et al. (1999). Quantitative analysis of earthworm burrow systems with respect to biological soil-structure regeneration after soil compaction. Biology and Fertility of Soils 28(3): 219-229. DOI: 10.1007/s003740050486

Lee CA, Lauenroth WK (1994) Spatial distributions of grass and shrub root systems in the shortgrass steppe. American Midland Naturalist 132(1): 117-123. DOI: 10.2307/2426206

Lee TC, Kashyap RL, Chu CN (1994) Building skeleton models via 3-D medial surface axis thinning algorithms. CVGIP: Graphical Models and Image Processing 56(6): 462-478. DOI:10.1006/ cgip.1994.1042

Legout A, Legout C, Nys C, et al. (2009) Preferential flow and slow convective chloride transport through the soil of a forested landscape (Fougères, France). Geoderma 151(3): 179-190. DOI:10.1016/j.geoderma.2009.04.002

Lin HS, McInnes KJ, Wilding LP, et al. (1996) Effective porosity and flow rate with infiltration at low tensions in a well-structured subsoil. Transactions of the ASAE 39(1): 131-135. DOI: 10.13031/2013.27490

Lu B, Zhang SL, Li K, et al. (2014) Distribution of soil macropores and their influence on saturated hydraulic conductivity in the Huoditang region of the Qinling Mountains. Aata Ecological Sinica 34(6): 1512-1519. DOI: 10.5846/stxb201210281493 (In Chinese)

Luo LF, Lin H, Li SC (2010) Quantification of 3-D soil macropore networks in different soil types and land uses using computed tomography. Journal of Hydrology 393(1): 53-64. DOI:10.1016/j.jhydrol.2010.03.031

Luo RY (1983) Forest soils (questions and methods). Beijing: Science Press. p 369. (In Chinese)

Luxmoore RJ, Jardine PM, Wilson GV, et al. (1990) Physical and chemical controls of preferred path flow through a forested hillslope. Geoderma 46: 139-154. DOI: 10.1016/0016-7061(90)90012-X

Martínez FSJ, Martín MA, Caniego FJ, et al. (2010) Multifractal analysis of discretized X-ray CT images for the characterization of soil macropore structures. Geoderma 156(1): 32-42. DOI:10.1016/ j.geoderma.2010.01.004

Marzen M, Iserloh T, Casper M C, et al. (2015) Quantification of particle detachment by rain splash and wind-driven rain splash. Catena 127: 135-141. DOI: 10.1016/j.catena.2014. 12. 023

Messing I, Alrikkson A, Johansson W (1997) Soil physical properties of afforested and arable land. Soil Use and Management 13: 209-217. DOI: 10.1111/j.1475-2743.1997. tb00588.x

Mooney SJ (2002) Three‐dimensional visualization and quantification of soil macroporosity and water flow patterns using computed tomography. Soil Use and Management 18(2): 142-151. DOI: 10.1111/j.1475-2743.2002.tb00232.x

Mooney SJ, Morris C (2008) A morphological approach to understanding preferential flow using image analysis with dye tracers and X-ray computed tomography. Catena 73(2): 204-211. DOI: 10.1016/j.catena.2007.09.003

Nanjing Hydraulic Research Institute (1999) Specification of soil test. Beijing: China Water & Power Press. p 556. (In Chinese)

Nobles MM, Wilding LP, Lin HS (2010) Flow pathways of bromide and Brilliant Blue FCF tracers in caliche soils. Journal of Hydrology 393(1): 114-122. DOI:10.1016/j.jhydrol. 2010.03.014

Noguchi S, Tsuboyama Y, Sidle RC, et al. (1997) Spatially distributed morphological characteristics of macropores in forest soils of Hitachi Ohta Experimental Watershed, Japan. Journal of Forest Research 2(4): 207-215. DOI: 10.1007/ BF02348317

Norgaard T, Moldrup P, Olsen P, et al. (2013) Comparative mapping of soil physical–chemical and structural parameters at field scale to identify zones of enhanced leaching risk. Journal of Environmental Quality 42(1): 271-283. DOI: 10.2134/jeq2012. 0105

Pagenkemper SK, Athmann M, Uteau D, et al. (2015) The effect of earthworm activity on soil bioporosity–Investigated with X-ray computed tomography and endoscopy. Soil and Tillage Research 146: 79-88. DOI: 10.1016/j.still. 2014.05.007

Perret J, Prasher SO, Kantzas A, et al. (1999) Three-dimensional quantification of macropore networks in undisturbed soil cores. Soil Science Society of America Journal 63(6): 1530-1543. DOI:10.2136/sssaj1999.6361530x

Pierret A, Capowiez Y, Belzunces L, et al. (2002) 3D reconstruction and quantification of macropores using X-ray computed tomography and image analysis. Geoderma 106(3): 247-271. DOI: 10.1016/S0016-7061(01)00127-6

Price K, Jackson CR, Parker AJ (2010) Variation of surficial soil hydraulic properties across land uses in the southern Blue Ridge Mountains, North Carolina, USA. Journal of Hydrology

383(3): 256-268. DOI: 10.1016/j.jhydrol.2009.12.041

Prosdocimi M, Cerdà A, Tarolli P (2016) Soil water erosion on Mediterranean vineyards: A review. Catena 141: 1-21. DOI: 10.1016/j.catena.2016.02.010

Ren BZ (2014) The formation mechanism of clay minerals in residual soil of emeishan basalt slope. Master Thesis, Kunming University of Science and Technology, Kunming, Yunnan. p24, 32. (In Chinese)

Rodrigo Comino J, Brings C, Lassu T, et al. (2015) Rainfall and human activity impacts on soil losses and rill erosion in vineyards (Ruwer Valley, Germany). Solid Earth 6(3): 823-837. DOI: 10.5194/se-6-823-2015

Rodrigo Comino J, Sinoga JDR, González JMS, et al. (2016a) High variability of soil erosion and hydrological processes in Mediterranean hillslope vineyards (Montes de Málaga, Spain). Catena 145: 274-284. DOI: 10.1016/j.catena.2016.06.012

Rodrigo Comino J, Iserloh T, Lassu T, et al. (2016b) Quantitative comparison of initial soil erosion processes and runoff generation in Spanish and German vineyards. Science of The Total Environment 565: 1165-1174. DOI: 10.1016/j.scitotenv. 2016.05.163

Rogasik H, Schrader S, Onasch I, et al. (2014) Micro-scale dry bulk density variation around earthworm (Lumbricus terrestris L.) burrows based on X-ray computed tomography. Geoderma 213: 471-477. DOI: 10.1016/j.geoderma.2013.08. 034

Schlather M, Huwe B (2005). A risk index for characterising flow pattern in soils using dye tracer distributions. Journal of contaminant hydrology 79(1): 25-44. DOI: 10.1016/j.jconhyd. 2005.05.005

Schmid B, Schindelin J, Cardona A, et al. (2010) A high-level 3D visualization API for Java and ImageJ. BioMed Central bioinformatics 11(1): 1-7. DOI: 10.1186/1471-2105-11-274

Schrader S, Rogasik H, Onasch I, et al. (2007) Assessment of soil structural differentiation around earthworm burrows by means of X-ray computed tomography and scanning electron microscopy. Geoderma 137(3): 378-387. DOI: 10.1016/j.geoderma.2006.08.030

Sheng F, Zhang LY, Wu D (2016) Review on research theories and observation techniques for preferential flow in unsaturated soil. Transactions of the Chinese Society of Agricultural Engineering 32(6): 1-10. DOI: 10.11975/j.issn. 1002-6819.2016. 06.001 (In Chinese)

Sidle RC, Noguchi S, Tsuboyama Y, et al. (2001) A conceptual model of preferential flow systems in forested hillslopes: evidence of self-organization. Hydrological Processes 15(10): 1675-1692. DOI: 10.1002/hyp.233

Sohrt J, Ries F, Sauter M, et al. (2014) Significance of preferential flow at the rock soil interface in a semi-arid karst environment. Catena 123: 1-10. DOI: 10.1016/j.catena.2014. 07. 003

Uchida T, Kosugi K, Mizuyama T (2001) Effects of pipeflow on hydrological process and its relation to landslide: a review of pipeflow studies in forested headwater catchments. Hydrological Processes 15(11): 2151-2174. DOI: 10.1002/hyp.281

Van Schaik N, Schnabel S, Jetten VG (2008) The influence of preferential flow on hillslope hydrology in a semi-arid watershed (in the Spanish Dehesas). Hydrological processes 22(18): 3844-3855. DOI:10.1002/hyp.6998

Watson KW, Luxmoore RJ (1986) Estimating macroporosity in a forest watershed by use of a tension infiltrometer. Soil Science Society of America Journal 50(3): 578-582. DOI: 10.2136/ sssaj1986.03615995005000030007x

Wiekenkamp I, Huisman JA, Bogena HR, et al. (2016) Spatial and temporal occurrence of preferential flow in a forested headwater catchment. Journal of Hydrology 534: 139-149. DOI: 10.1016/j.jhydrol.2015.12.050

Zhang C, Chen Y, Zhang YF, et al. (2016) Geohazard susceptibility evaluation in Zhaotong of Yunnan based on the multivatiate linear regression model. Hydrogeology andEngineering Geology 43(3):159-163. DOI: 10.16030/j.cnki.issn.1000-3665.2016.03.25 (In Chinese)

Zhang JM, Xu ZM, Pei YG (2012) Macropores in vadose zone of well vegetated slopes. Mountain Research 30(4): 439-449. DOI: 10.16089/j.cnki.1008-2786.2012.04.019 (In Chinese)

Zhang JM, Xu ZM (2013) A dye tracer experiment to study macropore flow paths in unsaturated zone under different vegetated communities in Maka Mountian, China. Journal of Jilin University (Earth Science Edition) 43(6): 1922-1935. DOI: 10.13278/j.cnki.jjuese.2013.06.028 (In Chinese)

Zhang JM, Xu ZM (2016) Dye tracer infiltration technique to investigate macropore flow paths in Maka Mountain, Yunnan Province. Journal of Central South University 23(8): 2101-2109. DOI: 10.1007/s11771-016-3266-y

Zhang YH, Niu JZ, Zhang MX, et al. (2016) Interaction Between Plant Roots and Soil Water Flow in Response to Preferential Flow Paths in Northern China. Land Degradation & Development. DOI: 10.1002/ldr.2592

Zhao CH, Gao JE, Huang YF, et al. (2016) Effects of vegetation stems on hydraulics of overland flow under varying water discharges. Land Degradation & Development 27: 748-757. DOI: 10.1002/ldr.2423

Zhou BB, Shao MN, Shao HB (2009) Effects of rock fragments on water movement and solute transport in a Loess Plateau soil. Comptes Rendus Geoscience 341(6): 462-472. DOI: 10.1016/j.crte.2009.03.009

Zhou X, Lin HS, White EA (2008) Surface soil hydraulic properties in four soil series under different land uses and their temporal changes. Catena 73(2): 180-188. DOI:10.1016/j.catena.2007.09.009

Zhou Y, Zhang J, Luo HS, et al. (2001) Tensile strength in lateral roots of Pinus and Cyclobalanopsis and its significance in maintaining slope stability in a shelter-forest system. Acta Phytoecological Sinica 25(1): 105-109 (In Chinese)

Xu ZM, Huang RQ, Tang ZG (2007) Engineering geological characteristics of the Touzhai landslide and its occurrence mechanisms. Geological Review 53(5): 691-698. DOI: 10.16509/j.georeview.2007.05.019 (In Chinese)

Xu ZM, Huang RQ (2011). The response of the groundwater in vegetated slopes in mountainous catchments to heavy rain events. Advances in Earth Science 26(6): 598-607 (In Chinese)